ACS OMEGA

Article

Cite This: ACS Omega 2019, 4, 8022−8030

http://pubs.acs.org/journal/acsodf

Study of the Partial Charge Transport Properties in the Molten Alumina via Molecular Dynamics

Aïmen E. Gheribi,*[,†] Alessandra Serva,[‡] Mathieu Salanne,[‡] Kelly Machado,[§] Didier Zanghi,[§] Catherine Bessada,[§] and Patrice Chartrand[†]

[†]Department of Chemical Engineering, Centre for Research in Computational Thermochemistry (CRCT)—Polytechnique Montréal, Box 6079, Station Downtown, Montréal, Québec, Canada H3C 3A7

[‡]CNRS, Physico-chimie des électrolytes et nanosystèmes interfaciaux, Phenix, Sorbonne Université, F-75005 Paris, France

[§]CEMHTI, CNRS UPR3079, 1D Avenue de la Recherche Scientifique, 45071 Orléans, France

ABSTRACT: Knowing the charge-transport properties of molten oxides is essential for industrial applications, particularly when attempting to control the energy required to separate a metal from its ore concentrate. Nowadays, in the context of a drastic increase of computational resources, research in industrial process simulation and their optimization is gaining popularity. Such simulations require accurate data as input for properties in a wide range of compositions, temperatures, and mechanical stresses. Unfortunately, due to their high melting points, we observe a severe lack of (reproducible) experimental data for many of the molten oxides. An alternative consists in using molecular dynamic simulations employing nonempirical force fields to predict the charge-transport properties of molten oxides and thus alleviate the lack of experimental data. Here, we study molten alumina using two polarizable force fields, with different levels of sophistication, parameterized on electronic structure calculations only. After validating the models against the experimental sets of density and electrical conductivity, we are able to determine the various ionic contributions to the overall charge transport in a wide range of temperatures.

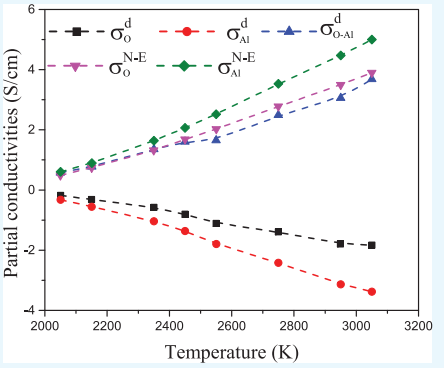

INTRODUCTION

Molten oxide systems, commonly referred to as slags, are of critical importance particularly in the domain of metallurgy. Indeed, slags are involved not only in the production of both ferrous and nonferrous metals but also in refining technologies, coal gasification, and continuous casting, to mention a few. A good knowledge of the thermodynamics, physical, charge-transport, and thermal transport properties of slags is needed for optimizing the industrial processes. Nowadays, due to economical as well as environmental issues, reducing the energy consumption of electric smelting processes and aluminium electrolysis is one of the most important challenges of the metallurgical industry. The energy needed for such processes is directly related to the partial ionic conductivity of each charged species within the slag. Unfortunately, there is a severe lack of experimental data for partial charge transport properties of slags, even for key industrial systems. Of course, this is detrimental when designing low-energy smelting processes. If we take the specific case of aluminium: despite the fact that it is the most abundant metal on earth, it is expensive, largely because of the amount of electricity used up in its extraction process. Indeed, aluminium is produced by the electrolysis of alumina, which is first dissolved in a molten cryolite-based electrolyte. Designing processes aimed at minimizing the overall energy consumption requires an accurate knowledge of not only the total conductivity molten Al_2O_3 but also the partial conductivity of all charges involved in the alumina electrolysis process as a function of temperature and composition. For molten alumina, many experimental data of total ionic conductivity are reported in the literature.[1−6] Yet, all these results were obtained via the 4-point probes method.[7] As pointed out by Schiefelbein et al.,[8] this technique is inaccurate and consequently large discrepancy is observed between each data set. For example, close to the melting point (2327 K), the total conductivity reported by Arkel et al.[6] is about 20 times larger than that reported by Wray and Neu.[5] As these data were measured with the same experimental method and in the same period (1960s−1970s), it is difficult to critically assess the total ionic conductivity by rejecting one or several data sets. The temperature dependence of the total ionic conductivity of molten Al_2O_3 is also in conflict. According to Elyutin et al.[4] and Wray and Neu,[5] the total conductivity increases very slightly with temperature, contrary to Arkel et al.,[6] who observed a significant temperature dependence of the conductivity. In principle, for molten oxides, the capillarity method would be the most accurate experimental technique,[8] but it was applied on some slags with a melting temperature much lower than that of alumina.[9−12] Partial conductivity is a key property to characterize current efficiency within an electrolysis cell. Unfortunately, no experimental data are

Received: April 17, 2019
Accepted: April 23, 2019
Published: May 2, 2019

DOI: 10.1021/acsomega.9b01110
ACS Omega 2019, 4, 8022−8030

reported either for Al^{3+} or for O^{2-}. Partial conductivity is a contribution of each ion to total conductivity. The ratio between partial and total conductivity is called the external transport number or transference number. The external transport numbers of ionic molten systems are in general measured via the Hittorf method[13] and occasionally with the so-called Moving boundary method.[14] The Hittorf method has been successfully applied to measure the cation external transport numbers for several pure molten salt compounds and some binaries.[15,16] For most molten oxides, due to their high melting points, the external transport numbers have never been measured. Note that most of the time, the external transport numbers are estimated from the diffusion coefficient via Nernst−Einstein (N−E) relationship. However, Nernst−Einstein equation is only valid when the ion cross-correlations can be neglected.[17] This is not the case for systems with strong short-range ordering leading to the formation of coordination complexes. In other words, Nernst−Einstein equation may be valid only for simple and fully dissociated oxides like MgO and CaO.

To alleviate conflicting and missing data on total ionic conductivity and the lack of experimental data on partial conductivity, with this work, we propose to predict the charge-transport properties of molten alumina by equilibrium molecular dynamics (EMD).

In prior works,[18−24] we have already demonstrated that EMD, using interaction potentials fitted from first-principle density functional theory (DFT) calculations only, can predict the thermodynamic, dynamic, charge-transport, thermal transport, and structural properties of molten salts and oxides with appreciable accuracy. In a recent work,[25] we have proposed a new formalism to extend the EMD capabilities for the prediction of partial charge transport properties of molten salts. Considering the same formalism, we propose to study the partial charge transport properties within molten Al_2O_3. The predicted total ionic conductivity and density are compared with the available experimental data to evaluate the reliability of the EMD simulations, even if a large dispersion is observed between different data sets. Furthermore, to explain the microscopic aspect of the charge-transport properties, we focus on the correlation between the total and partial conductivity, the local structure, and the charge−charges effect.

METHODS

Molecular Dynamic Simulations. The simulations are performed with the PIM code. Details on PIM can be found in.[26,27] The procedure employed to perform the EMD simulations is the same as that in our prior work.[25] Two sets of interionic potentials are used in this work. The first one (EMD-1 in the following) is taken from Machado et al.[28]

The interionic potentials consists of a Coulombic repulsion term coupled with a Born−Mayer type interaction term, together with dispersion and polarization interaction terms[29]

$$V = \sum_{i<j}\left[\frac{q_i q_j}{r_{ij}} + B_{ij}\, e^{-\alpha_{ij} r_{ij}} \underbrace{f_{ij}^{6}(r_{ij})\frac{C_{ij}^{6}}{r_{ij}^{6}} - f_{ij}^{8}(r_{ij})\frac{C_{ij}^{8}}{r_{ij}^{8}}}_{V_{\mathrm{disp}}}\right] + V_{\mathrm{pol}}(\alpha_i, p_i) \quad (1)$$

V_{disp} describes the dispersion interactions, with C_{ij}^6 and C_{ij}^8 as the dispersion coefficients. It accounts for the short-range penetration correction to the asymptotic multipole expansion of dispersion through Tang−Toennies damping functions, $f_{ij}^{(n)}$, expressed as[30]

$$f_{ij}^{(n)} = 1 - e^{-b_{ij}^{n} r_{ij}} \sum_{k=0}^{n} \frac{(b_{ij}^{n} r_{ij})^{n}}{k!} \quad (2)$$

V_{pol} is a polarization term describing the distortion of the electronic density in response to electric fields due to all other ions. The dipoles are determined at each simulation time step by minimizing the total polarization energy. The potential parameters are found ab initio by fitting the dipoles and forces to those obtained by DFT calculations. The second interionic potential (EMD-2) is taken from Ishii et al.[31] It differs from the first one in two aspects. First, it includes many-body effects on the short-range repulsion between Al and O ions through the introduction of additional degrees of freedom that mimic the change of radius and shape of the electronic cloud of the oxide ion. Second, the parameters were derived from a different set of DFT calculations (albeit conducted at the same level of approximation). Note that the inclusion of additional many-body effects is expected to improve the predictive ability of the potential, but it comes at a cost: the simulations are slower by a factor 3−4 with respect to EMD-1. With both potentials, the simulations were carried in the range of $2050 \leq T \leq 3050$ K by varying the temperature by a step of 100 K. The total number of ions in the simulation box is, for all temperatures, 540 (216 Al^{3+} and 324 O^{2-}). The volume of the system was determined by a prior simulation in the isobaric−isothermal statistical ensemble (NPT) at the corresponding temperature and at $P = 10^5$ Pa. Then, starting with a thermally equilibrated initial configuration (generated by NPT simulation), another series of simulations was performed on the canonical statistical ensemble (NVT). The volume of the simulation box for NVT simulations was fixed to the average volume determined by the NPT simulations. The temperature was controlled with Nosé−Hoover thermostat[32] for both NPT and NVT simulations. For the NPT simulations, the pressure was controlled by an extension of the Martyna barostat.[33] The thermostat and barostat relaxation times were both 0.5 ps. The equations of motion were integrated using the velocity Verlet algorithm,[34] with a time step of 1 fs. The total simulation time was 1.5 ns for EMD-1 and 0.75 ns for EMD-2 for the NPT and 5 ns for both potentials for NVT simulations. Lastly, all simulations were performed using periodic boundary conditions and minimum image convention.

Theory. From the simulated phase trajectory, we calculated first the self-diffusion coefficient under periodic boundary conditions from the slope of the mean-squared displacements (MSD) versus time

$$D_i^{\mathrm{PBC}} = \lim_{t\to\infty} \frac{1}{6t}\langle |\delta \mathbf{r}_a(t)|^2 \rangle \quad (3)$$

where $\delta \mathbf{r}_a$ is the displacement of a given ion of species i in time t. This value depends on the box size, so the correction proposed by Yeh and Hummer[35] was included to obtain the correct self-diffusion coefficient D_i^0. To do so, it is necessary to estimate the shear viscosity of the fluid, which can be obtained from the integral over time of the autocorrelation function of the anisotropic elements of the stress tensor $\sigma_{\alpha\beta}$

$$\eta = \beta V \int_0^{\infty} \langle \sigma_{\alpha\beta}(0)\sigma_{\alpha\beta}(t)\rangle \, \mathrm{d}t \quad (4)$$

DOI: 10.1021/acsomega.9b01110
ACS Omega 2019, 4, 8022−8030

Table 1. Total and Partial Charge Transport Properties of Molten Al_2O_3 Calculated from EMD-1[a]

T		ρ	σ	σ^{N-E}	σ_i	$10^6 \times D_i^0$	t_i	t_i^{N-E}
	Tot.	3.08	0.50	0.41				
2050 K	O^{2-}				0.30	0.97	0.54	0.46
	Al^{3+}				0.26	0.75	0.46	0.54
	Tot.	3.06	0.87	0.77				
	O^{2-}				0.44	1.88	0.52	0.45
	Al^{3+}				0.40	1.50	0.48	0.55
	Tot.	3.04	2.13	1.63				
	O^{2-}				0.95	4.45	0.53	0.47
	Al^{3+}				0.84	3.40	0.47	0.53
	Tot.	3.03	2.80	2.41				
	O^{2-}				1.23	6.46	0.53	0.44
	Al^{3+}				1.09	5.58	0.47	0.56
	Tot.	3.00	2.60	3.19				
	O^{2-}				1.40	8.94	0.52	0.44
	Al^{3+}				1.30	7.71	0.48	0.56
	Tot.	2.97	4.18	4.86				
	O^{2-}				2.49	14.65	0.53	0.43
	Al^{3+}				2.21	12.99	0.47	0.57
	Tot.	2.93	5.60	6.21				
	O^{2-}				3.64	20.37	0.53	0.43
	Al^{3+}				3.22	18.06	0.47	0.57
	Tot.	2.91	7.50	7.18				
	O^{2-}				4.44	24.61	0.53	0.43
	Al^{3+}				3.94	21.69	0.47	0.57

[a]The density (ρ), total conductivity (σ), partial conductivity (σ_is), self-diffusion coefficients (D_i^0's), and external transport numbers (t_is) are given in the range 2050 K $\leq T \leq$ 3050 K. The conductivity and the external transport numbers derived from Nernst−Einstein approximation (N−E) are also reported to quantify the ion's correlation effect upon the charge transport. The standard error associated with each property is calculated by the error block averaging method[37,38] and reported only on the figures if they are significant. Units are as follows: ρ is in g cm^{-3}, σ and σ_i are in S cm^{-1}, and D^0 is expressed in cm^2 s^{-1}.

where $\beta = 1/k_B T$ (k_B being the Boltzmann constant) and V the equilibrium volume. An average over five independent components of the stress tensor is performed to improve the statistics. The MSD was fitted in the long time motion region ($t \geqslant 10$ ps) to ensure linearity of the MSD with time and thus avoid collision-free motion.

The total ionic conductivity is obtained from the slope of the total MSD of the charge density versus time[36]

$$\sigma = \frac{\beta e^2}{V} \lim_{t\to\infty} \frac{1}{6t} \left\langle \left| \sum_a Z_a \delta \mathbf{r}_a(t) \right|^2 \right\rangle \tag{5}$$

where Z_i is the formal charge of ion i. The most important aspect of this paper is the study of the partial ionic conductivity of molten oxides. The partial ionic conductivity, σ_i, results from the decomposition of the total ionic conductivity into individual ion's contribution, i.e.,: $\sigma = \sum_i \sigma_i$. Most of the time, in the literature, instead of the partial conductivity, the external transport number $t_i = \sigma_i/\sigma$ is used to quantify the relative contribution of each ion to the total conductivity. The partial conductivity of i can be formulated as[25]

$$\sigma_i = \frac{\beta e^2}{V} \lim_{t\to\infty} \frac{1}{6t} \left\langle Z_i^2 \Delta_i^2(t) + \sum_{j\neq i} \omega_{i-j}^i Z_i Z_j \Delta_i(t) \Delta_j(t) \right\rangle \tag{6}$$

where $\Delta_i(t) = N_i^{-1} \sum_{a\in i} \delta \mathbf{r}_a(t)$ and ω_{i-j}^j quantify the interferences from other species on ion i, i.e., the mutual effect upon the total conductivity generated by various $i-j$ pairs. Note that the ω_{i-j} parameters are subjected to the constraint: $\omega_{i-j}^i + \omega_{i-j}^j = 2$. Similar to the case of conventional solvents, for simple molten ionic compounds, we have shown that the anion−cation interferences help to increase only the external transport number (partial ionic conductivity) of the cation at the expense of the anion. Indeed, in conventional solvents, the transport numbers are defined in the framework of the solvent, which is usually considered immobile in the presence of an electric field. If there is no solvent, it is rather natural to confer an equivalent role to the anions, since it is the cationic composition that mostly varies. When ions are strongly correlated and form coordination complexes, both cation and anions have similar interference contributions upon the partial conductivity and thus[25]

$$\begin{cases} \omega_{O^{2-}-Al^{3+}}^{O^{2-}} = 1 \\ \omega_{O^{2-}-Al^{3+}}^{Al^{3+}} = 1 \end{cases} \tag{7}$$

It is important to note that the specific case of $\omega_{i-j}^j = 0$ is not equivalent to Nernst−Einstein approximation because it accounts for correlations that may occur between same type of ions. Indeed, Nernst−Einstein (N−E) approximation assumes that the motion of ions within an electrolyte are uncorrelated. In this case, the ionic mobility is proportional to the self (tracer) diffusion coefficient and the partial conductivity of species i can be written as

$$\sigma_i^{N-E} = \beta e^2 Z_i^2 \rho_i D_i^0 \tag{8}$$

where ρ_i is the density number of the species of type i. Then, the total ionic conductivity in Nernst−Einstein approximation is

DOI: 10.1021/acsomega.9b01110
ACS Omega 2019, 4, 8022−8030

Table 2. Total and Partial Charge Transport Properties of Molten Al_2O_3 Calculated from EMD-2[a]

T		ρ	σ	σ^{N-E}	σ_i	$10^6 \times D_i^0$	t_i	t_i^{N-E}
	Tot.	2.95	1.17	1.16				
2050 K	O^{2-}				0.62	2.84	0.53	0.47
	Al^{3+}				0.55	2.19	0.47	0.53
	Tot.	2.93	1.58	1.79				
2150 K	O^{2-}				0.84	4.55	0.53	0.46
	Al^{3+}				0.74	3.58	0.47	0.54
	Tot.	2.90	2.76	3.23				
2350 K	O^{2-}				1.46	8.89	0.53	0.45
	Al^{3+}				1.30	7.35	0.47	0.55
	Tot.	2.88	3.26	4.03				
2450 K	O^{2-}				1.73	11.64	0.53	0.45
	Al^{3+}				1.53	9.61	0.47	0.55
	Tot.	2.86	3.33	4.88				
2550 K	O^{2-}				1.76	14.65	0.53	0.44
	Al^{3+}				1.57	12.26	0.47	0.56
	Tot.	2.82	5.03	6.74				
2750 K	O^{2-}				2.66	21.86	0.53	0.44
	Al^{3+}				2.37	18.62	0.47	0.56
	Tot.	2.79	6.16	8.51				
2950 K	O^{2-}				3.26	29.84	0.53	0.44
	Al^{3+}				2.90	25.64	0.47	0.56
	Tot.	2.77	7.40	9.44				
3050 K	O^{2-}				3.92	34.36	0.53	0.44
	Al^{3+}				3.48	29.69	0.47	0.56

[a]The density (ρ), total conductivity (σ), partial conductivity (σ_is), self-diffusion coefficients (D_i^0s), and external transport numbers (t_is) are given in the range $2050 \leq T \leq 3050$ K. The conductivity and the external transport numbers derived from Nernst−Einstein approximation (N−E) are also reported to quantify the ion's correlation effect upon the charge transport. The standard error associated with each property is calculated by the error block averaging method[37,38] and reported only on the figures if they are significant. Units are as follows: ρ is in g cm^{-3}, σ and σ_i are in S cm^{-1}, and D^0 is expressed in cm^2 s^{-1}.

given by $\sigma^{N-E} = \sum_i \sigma_i^{N-E}$. The calculated density and the total and partial charge transport properties of the Al_2O_3 molten system are provided in Tables 1 and 2 for the EMD-1 and EMD-2, respectively. The standard error associated with each property is calculated by the error block averaging method.[37,38] A total of 15 blocks were considered for NPT simulations and 25 blocks for NVT. The number of blocks is proportional to the simulation time and obtained after a convergence test. In the following, for clarity purposes, the errors are only displayed on the figures if they are significant.

RESULTS AND DISCUSSION

In Figure 1, the calculated density as a function of temperature is compared with the available experimental data and the recent CALPHAD assessment proposed by Robelin and Chartrand.[39] The agreement obtained with EMD-2 is overall very good, particularly with respect to the most recent experimental data sets, which are the ones by Paradis et al.[41] and Langstaff et al.[46] The predicted thermal expansion, which is 6.5×10^{-5} K^{-1} for this potential, is also in good agreement with these data. The values are also consistent with the ones obtained from the analysis of the density of multicomponents molten oxides systems via interpolation methods.[48,49] In the case of EMD-1, the density is overestimated by ≈4% over the whole temperature range. Such an error is of the same order of magnitude as the larger discrepancies between the various experimental data, which shows that this potential remains almost quantitative.

The experimental and simulated viscosities are displayed in Figure 2. As for the density, strong discrepancies are observed between various experimental data sets. In particular, the data

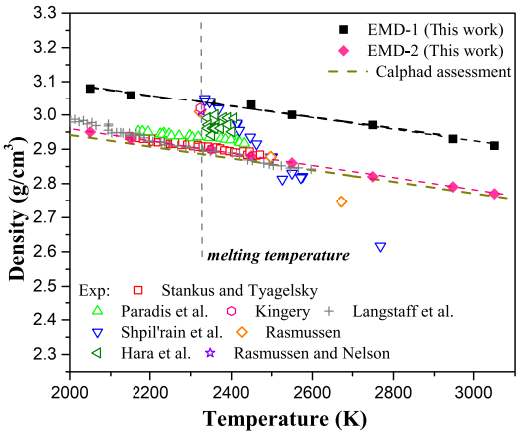

Figure 1. Calculated density of molten Al_2O_3 with the potential 1 and 2 (solid squares and solid diamond connected with dashed lines) as a function of temperature in comparison with the experimental data (open symbols) and CALPHAD assessment[39] (dash-dot line). Experimental data are referenced as follows: Stankus and Tyagelsky[40] (open squares), Paradis et al.[41] (open up-triangles), Shpil'rain et al.[42] (open down-triangles), Rasmussen[43] (open diamonds), Rasmussen and Nelson[44] (open stars), Hara et al.[45] (open left-triangles), Langstaff et al.[46] (cross), and Kingery[47] (open hexagon). The melting temperature of alumina is indicated by a vertical dashed line. The statistical error of EMD simulations, obtained via block method, is found to be negligible, about 0.1%; they are thus not reported in the figure.

from Bates et al.[52] clearly differ a lot from those of others. We observe that above the melting point, the EMD-2 gives values

DOI: 10.1021/acsomega.9b01110
ACS Omega 2019, 4, 8022−8030

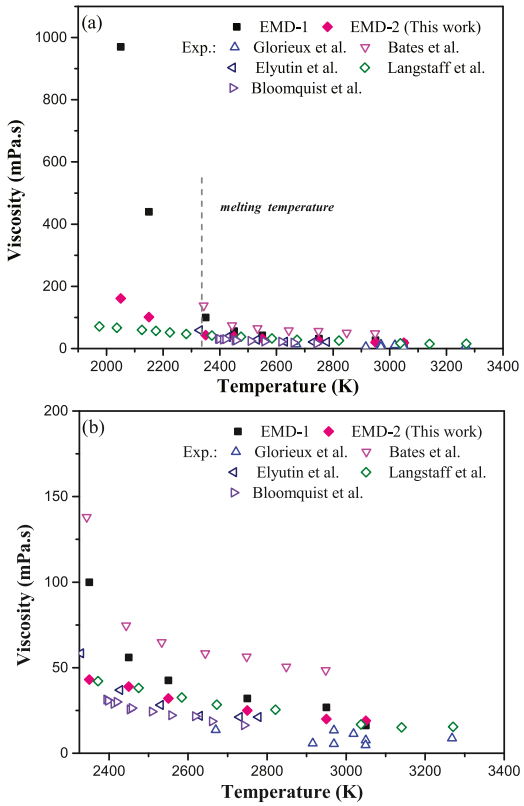

Figure 2. Calculated shear viscosity of molten Al_2O_3 (solid symbols) as a function of temperature in comparison with experimental data (open symbols). The top (a) represents the viscosity of both stable and supercooled molten Al_2O_3 at a temperature up to 350 K below melting, whereas the bottom (b) represents the viscosity of stable molten Al_2O_3 only, i.e., above the melting temperature. Experimental data are referenced as follows: Glorieux et al.,[50] Elyutin et al.,[51] Langstaff et al.,[46] Bates et al.,[52] and Blomquist et al.[53] The melting temperature of alumina is indicated by a vertical dashed line. The statistical error of EMD simulation is found to be negligible and not reported in the figure.

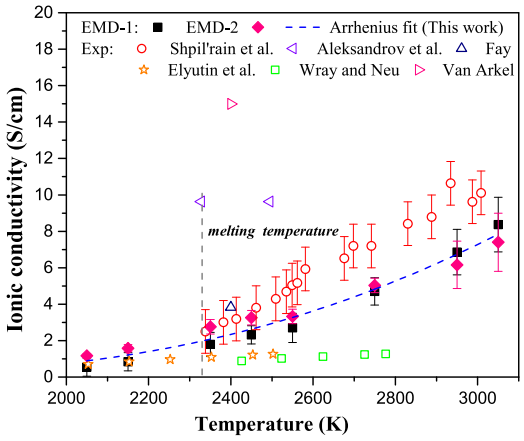

Figure 3. Calculated ionic conductivity of molten Al_2O_3 (solid squares connected with dashed lines) as a function of temperature in comparison with experimental data (open symbols). The dash-dot line represents the Arrhenius equation fitting curve of EMD data. Experimental data are referenced as follows: Shpil'rain et al.[1] (open circles), Aleksandrov et al.[2] (open left-triangles), Fay.[3] (open up-triangle), Elyutin et al.[4] (open stars), Wray and Neu[5] (open squares), and Arkel et al.[6] (open right-triangles). The melting temperature of alumina is indicated by a vertical dashed line.

that lie within the other experimental data, showing that this model predicts correctly the fluidity of the melt. The EMD-1 values seem to be slightly large, an effect that may arise from the discrepancy already observed for the density. At temperatures lower than the melting point, in the supercooled regime, the EMD-2 deviates substantially from the only available data from Langstaff et al.,[46] but this may be due to the sampling of different structures, since the system is metastable in this range.

The calculated ionic conductivity as a function of temperature is represented in Figure 3, where it is compared with the available experimental data. As for the other physical properties, a very large discrepancy is observed between different experimental data sets (more than 1 order of magnitude in the case of molten alumina). Of course, this is due to experimental limitations when measuring electrical resistivity at high temperature. From a practical point of view, it is precisely in such situations that first-principles-based EMDs take their full meaning. Indeed, given the apparent large discrepancy between each data set, it is at first glance difficult to discuss the reliability of EMD calculations. Nonetheless, here we clearly claim that in such situations, EMD data should be considered as a reference, as the method has already proven its high predictive capability for several dynamic and transport properties for both simple and complex molten ionically bonded systems.[18−22,25] Our calculated ionic conductivities are in good agreement with those of the two models. Both agree well with some data sets for both liquid and undercooled Al_2O_3: specifically, those reported by Shpil'rain et al.[1] from melting temperature up to 3000 K, and those reported by Elyutin et al.[4] below the melting temperature as low as 2050 K. Experimental data reported by Aleksandrov et al.[2] and Arkel[6] are much higher than the other data sets and EMD calculations as well. The experimental data reported by Wray and Neu[5] are very close to those of Elyutin et al.[4] in the vicinity of the melting temperature, and thus in good agreement with our EMD predictions, but they are almost temperature independent, leading to a large discrepancy between EMD and Shpil'rain et al.'s[1] data at higher temperature. The predicted temperature dependence of the ionic conductivity of molten Al_2O_3 follows a linear Arrhenius behavior, i.e., $\sigma \propto e^{-E_a/RT}$, with an activation energy of E_a = 153.7 kJ mol^{-1}, as determined from EMD-1. The ionic conductivity of molten Al_2O_3 is relatively small in comparison that observed for simple oxides such as MgO, CaO, or MnO;[54] it can differ by at least 1 order of magnitude. This large gap is clearly due to differences in the local structure of the liquid: simple molten oxides consist of fully dissociated ions, whereas molten alumina O^{2-} and Al^{3+} form structural complexes that would drastically decrease the ion's mobility. To put it in a nutshell, in the case of molten Al_2O_3, and more generally for slags, the reliability of the predictions of ionic conductivity goes hand in hand with the accurate description of the local structure. Few experimental data characterizing the local structure of Al_2O_3 liquid are reported in the literature. In fact, only the total structure factor was experimentally determined by Ansell et al. via X-ray synchrotron radiation[55] and by Landron et al.[56,57] In addition to the structure factor, the average coordination number of oxygen for aluminium was also measured by NMR technique.[58−60]

In Figure 4, the calculated X-ray and neutron-weighted structure factors are compared between the interaction potentials EMD-1 and EMD-2. They are determined using

DOI: 10.1021/acsomega.9b01110
ACS Omega 2019, 4, 8022−8030

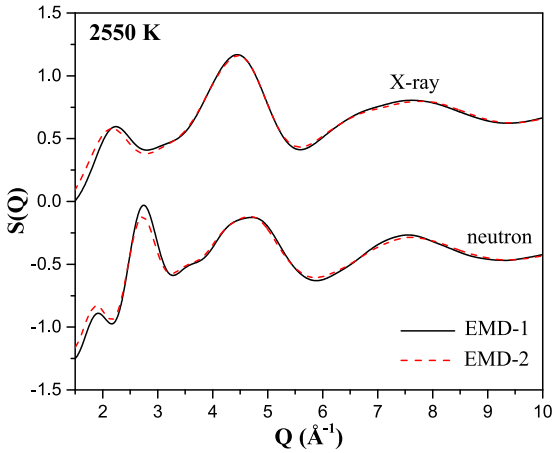

Figure 4. Calculated X-ray and neutron-weighted total structure factors for liquid Al_2O_3 at 2550 K.

$$S(k) = 1 + \frac{\sum_\alpha \sum_\beta c_\alpha c_\beta w_\alpha(k) w_\beta^*(k)[S_{\alpha\beta}(k) - 1]}{|\sum_\alpha c_\alpha w_\alpha(k)|^2} \quad (9)$$

where k is the scattering vector magnitude, c_α is the atomic fraction (of chemical species α), and w_α is the atomic form factor in the case of X-ray or the coherent neutron scattering length. $S_{\alpha\beta}$ is the partial structure factor, obtained from the partial radial distribution functions by performing a Fourier transform

$$S_{\alpha\beta}(k) = 1 + \frac{4\pi\rho}{k} \int_0^\infty r[g_{\alpha\beta}(r) - 1]\sin(kr)\, dr \quad (10)$$

where ρ is the atomic number density of the glass. The similarity between the structure factors obtained for EMD-1 and EMD-2 shows that the two models yield very similar structures for the liquid. The results are in good agreement with previous experiments[55,56] and simulations performed with a previous polarizable model, which was also fitted on DFT reference data (albeit in the local-density approximation approximation).[61−63]

The calculated and experimental average coordination numbers of Al about Al, n_{Al-Al}, are almost identical: 9.87 and 9.60 for EMD-1 and EMD-2, respectively vs 9.47 for the experiments. [The average coordination number is calculated by the integration of RDF: $n_{ij} = 4\pi\rho_j \int_0^{r_{min}} g_{ij} r^2\, dr$, where ρ is the number density and r_{min} is the position of the first minimum.] Similarly, the coordination number of oxygen for aluminium n_{O-Al} is 4.9 and 4.7 for EMD-1 and EMD-2, respectively, which compares well with the experiment-derived values of 4.2 ± 0.3 reported by Landron et al.,[56] 4.4 ± 1.0 reported by Ansell et al.[55] and 4.5 from NMR work of Florian et al.[58] It is important to note that a strong charge ordering is apparent in molten Al_2O_3. From the simulations, a closer look at the local structure within molten alumina can be obtained through the analysis of the distribution of coordination numbers. The calculated probabilities of coordination numbers of O^{2-} about Al^{3+} are represented in Figure 5. According to our EMD-1 simulations, molten Al_2O_3 has 28% 4-fold coordinated, 53% 5-fold coordinated, and 19% 6-fold coordinated aluminium atoms. This contradicts the generally accepted consensus where the mean coordination number is dominated not by 5-fold but rather 4-fold coordinated Al^{3+} leading to a local structure mainly formed of a tetrahedral network. This consensus originates from the interpretation by Ansell et al.[55] of their total structure factor measured by X-ray synchrotron radiation. The NMR experiments are less

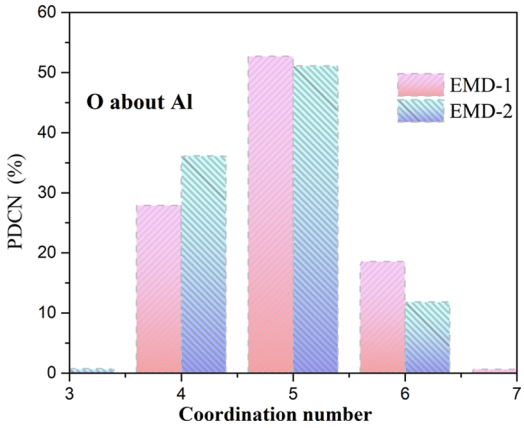

Figure 5. Calculated probability of coordination numbers of oxygen about aluminium at 2550 K obtained with both potentials.

categorical about the Al^{3+} coordination number, suggesting the presence of 4-, 5-, and 6-fold sites with an average coordination number estimated close to 4.5,[58,59] whereas our calculated Al^{3+} average coordination is 4.9. However, the present EMD calculations tend to overestimate the amount of 5-fold coordinated Al^{3+} at the expense of 4-fold coordinated Al^{3+}.

The ratios σ^{N-E}/σ and σ_i^{N-E}/σ_i are known, respectively, as the total and the partial Haven ratios (H); they account for multiple-ion correlation effect[64,65] upon the ionic conductivity. Haven ratios equal to 1 mean that the ions are noncorrelated and therefore the charge transport should strictly obey Nernst−Einstein law. In molten alumina, the ions are strongly correlated, leading to a collective ion migration, which explains why in the present work the total Haven ratio is found to deviate from unity (see Tables 1 and 2). However, the total Haven ratio is found to be less than one (about 0.75 for EMD-1 at 2050 K).

Contrary to the total Haven number, the partial haven number is closer to unity and the external transport number of both O^{2-} and Al^{3+} is close to 0.5, indicating that they are evolving within coordination complexes, with a negligible amount of free ionic species. To validate the ansatz formulated in our previous work,[25] given in eq 7 for systems showing a strong short-range ordering, let us consider the inverse situation and calculate what would be the external transport if O^{2-} and Al^{3+} were not complexed. In this case, the interference coefficients are written as[25]

$$\begin{cases} \omega_{O^{2-}-Al^{3+}}^{O^{2-}} = 0 \\ \omega_{O^{2-}-Al^{3+}}^{Al^{3+}} = 2 \end{cases} \quad (11)$$

i.e., the interference only increases the cations' mobility at the expense of anions'. In this case, we found that $t_{Al^{3+}} \simeq 0.74$ for all temperatures (EMD-1). This value matches exactly the external transport number expected for fully dissociated mixtures given by[16]

$$t_+ = \frac{r\_Z_+}{r_+Z\_ + r\_Z_+} \quad (12)$$

where $r_{+(-)}$ is the cation (anion) radius ($r_{O^{2-}} = 1.26$ Å and $r_{Al^{3+}} = 0.67$ Å[66]) and z the ion charge. This confirms not only the ansatz proposed in our previous work[25] for both complex and

DOI: 10.1021/acsomega.9b01110
ACS Omega 2019, 4, 8022−8030

dissociated systems (eqs 6 and 8) but also the reliability of EMD calculations in predicting external transport numbers.

Finally, it is worth noting that the two models (EMD-1 and EMD-2) provide similar electrical conductivities, whereas EMD-2 yields a significantly lower conductivity. This also reflects on the diffusion coefficients of both species, which are larger for EMD-2. This result suggests that the correlation may differ in magnitude between the two potentials. To test this, we followed the analysis of Kashyap et al.,[67] in which the total conductivity is split between all its various contributions. First, two Nernst−Einstein terms σ_i^{N-E} terms, which reflect the uncorrelated diffusion of the ions, and then three contributions arising from the correlations

$$\sigma_{Al}^{d} = \frac{\beta e^2}{V} \lim_{t\to\infty} \frac{1}{6t} \langle Z_{Al}^2 \Delta_{Al}^2(t) \rangle - \sigma_{Al}^{N-E} \quad (13)$$

$$\sigma_{O}^{d} = \frac{\beta e^2}{V} \lim_{t\to\infty} \frac{1}{6t} \langle Z_{O}^2 \Delta_{O}^2(t) \rangle - \sigma_{O}^{N-E} \quad (14)$$

$$\sigma_{O-Al}^{d} = \frac{\beta e^2}{V} \lim_{t\to\infty} \frac{1}{6t} \langle 2.0 Z_{Al} Z_{O} \Delta_{Al}(t) \Delta_{O}(t) \rangle \quad (15)$$

These five quantities are shown for all temperatures in Figure 6. First, we observe that they follow the same trend as in the case of room-temperature ionic liquids and molten salts discussed in the work of Kashyap et al.,[67] i.e., large cancellations occur between the self terms and the ones arising from correlations. Second, from the quantitative point of view, the magnitude of the terms varies consequently between EMD-1 and EMD-2. Indeed, the term arising from the correlations between O and Al atoms (green line) is the only one to take similar values between the two models. All other partial terms are increased by roughly 50%. As a consequence, similar ionic conductivity between the two models can be seen as a coincidence rather than a generic future.

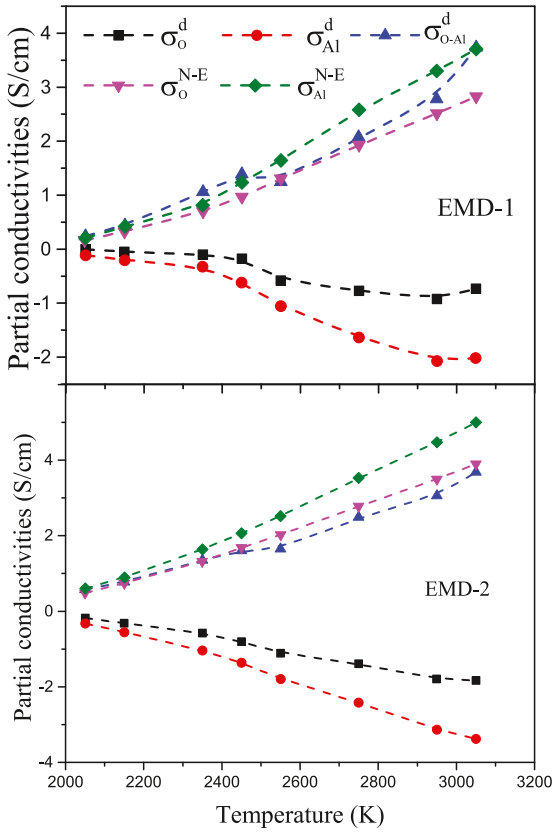

Figure 6. Comparison between partial conductivities: σ_{Al}^d, σ_O^d, and σ_{O-Al}^d with Nernst−Einstein partial conductivity for O (σ_O^{N-E}) and Al (σ_{Al}^{N-E}) simulated with both EMD-1 and EMD-2 potentials.

CONCLUSIONS

In summary, the partial charge transport properties of molten alumina were studied via first-principle-parameterized equilibrium molecular dynamics. The EMD predictions for both total and partial ionic conductivities were found to be reliable. Although the polarizable model correctly predicts the properties, the agreement is further improved by introducing additional many-body effects in the short-range repulsion potential. A correlation between the local structure and the total and partial transport properties has been clearly established. Hopefully, this work will open doors to the study of partial charge transport properties within complex slag systems, for which experimental data are desperately lacking.

AUTHOR INFORMATION

Corresponding Author

*E-mail: aimen.gheribi@polymtl.ca.

ORCID

Aïmen E. Gheribi: 0000-0002-5443-2277
Alessandra Serva: 0000-0002-7525-2494
Mathieu Salanne: 0000-0002-1753-491X
Kelly Machado: 0000-0001-6045-5734

Notes

The authors declare no competing financial interest.

ACKNOWLEDGMENTS

This research was supported by funds from the Natural Sciences and Engineering Research Council of Canada (NSERC), Rio Tinto Aluminium, Alcoa, Hydro Aluminium, Constellium. Computations were made on the supercomputer Briaré at the Université de Montréal, managed by Calcul-Québec and Compute Canada.

REFERENCES

(1) Shpil'rain, E. E.; Kagan, D. N.; Barkhatov, L. S.; Zhmakin, L. I. Experimental <tep-common:author-query>AQ2: Please provide a DOI number for ref 1 or indicate if one doesn’t exist.</tep-common:author-query>Study of the Electric Conductivity of Molten Aluminum Oxide at Temperatures to 3000 K. *Teplofiz. Vys. Temp.* **1976**, *14*, 948−952.

(2) Aleksandrov, V. I.; Osiko, V. V.; Tatarintsev, V. M. Electrical Conductivity of Aluminum Oxide in the Molten State. *Izv. Akad. Nauk SSSR, Neorg. Mater.* **1972**, *8*, 956−957.

(3) Fay, H. The Electrical Conductivity of Liquid Al2O3 (Molten Corundum and Ruby). *J. Phys. Chem.* **1966**, *70*, 890−893.

(4) Elyutin, V. P.; Mitin, B. S.; Nagibin, Y. A. Electrical Conductivity of Molten Aluminum Oxide. *Izv. Akad. Nauk SSSR, Neorg. Mater.* **1971**, *7*, 880−881.

(5) Wray, J. H.; Neu, J. T. Refractive Index of Several Glasses as a Function of Wavelength and Temperature*. *J. Opt. Soc. Am.* **1969**, *59*, 774−776.

(6) Arkel, A. V.; Flood, E. A.; Bright, N. F. H. The Electrical Conductivity of Molten Oxides. *Can. J. Chem.* **1953**, *31*, 1009−1019.

(7) Silný, A.; Haugsdal, B. Electrical Conductivity Measurements of Corrosive Liquids at High Temperatures. *Rev. Sci. Instrum.* **1993**, *64*, 532−537.

DOI: 10.1021/acsomega.9b01110
ACS Omega 2019, 4, 8022−8030

(8) Schiefelbein, S. L.; Fried, N. A.; Rhoads, K. G.; Sadoway, D. R. A High-Accuracy, Calibration-Free Technique for Measuring the Electrical Conductivity of Liquids. *Rev. Sci. Instrum.* **1998**, *69*, 3308−3313.
(9) Bauke, F. G. K.; Braun, J.; Roeth, G.; Werner, R. D. Accurate Conductivity Cell for Molten Glasses and Salts. *Glastech. Ber.* **1989**, *62*, 122−123.
(10) Baucke, F. G. K.; Werner, R. D. Mixed Alkali Effect of Electrical Conductivity in Glass-Forming Silicate Melts. *Glastech. Ber.* **1989**, *62*, 182−186.
(11) Pastukhov, E. A.; Esin, O. A.; Chuchmarev, S. K. Electric Conductivity of Silicate Melts Containing Iron Oxides. *Elektrokhimiya* **1966**, *2*, 209−215.
(12) Degtyarev, V. S.; Reznichenko, V. A.; Denisov, S. I.; Zobov, E. I.; Nerubashchenko, V. V. Measurement of the Electrical Conductivity of Highly Conductive Slags. *Zavod. Lab.* **1969**, *35*, No. 64.
(13) McCann, M. P. Physical Chemistry CD (Laidler, Keith James; Meiser, John H.; Sanctuary, Bryan C.). *J. Chem. Educ.* **2003**, *80*, No. 489.
(14) Lonergan, G. A.; Pepper, D. C. Transport Numbers and Ionic Mobilities by the Moving Boundary Method. *J. Chem. Educ.* **1965**, *42*, No. 82.
(15) Klemm, A. Transport Properties of Molten Salts. *Molten Salt Chem.* **1964**, 535−606.
(16) Sundheim, B. R. In *Fused Salts*; McGraw-Hill, 1964; p 464.
(17) Harris, K. R. Relations between the Fractional Stokes-Einstein and Nernst−Einstein Equations and Velocity Correlation Coefficients in Ionic Liquids and Molten Salts. *J. Phys. Chem. B* **2010**, *114*, 9572−9577.
(18) Gheribi, A. E.; Salanne, M.; Chartrand, P. Thermal Transport Properties of Halide Solid Solutions: Experiments vs Squilibrium Molecular Dynamics. *J. Chem. Phys.* **2015**, *142*, No. 124109.
(19) Gheribi, A. E.; Salanne, M.; Chartrand, P. Formulation of Temperature-Dependent Thermal Conductivity of NaF, B-Na3AlF6, Na5Al3F14, and Molten Na3AlF6 Supported by Equilibrium Molecular Dynamics and Density Functional Theory. *J. Phys. Chem. C* **2016**, *120*, 22873−22886.
(20) Gheribi, A.; Corradini, D.; Dewan, L.; Chartrand, P.; Simon, C.; Madden, P.; Salanne, M. Prediction of the Thermophysical Properties of Molten Salt Fast Reactor Fuel from First-Principles. *Mol. Phys.* **2014**, *112*, 1305−1312.
(21) Gheribi, A. E.; Torres, J. A.; Chartrand, P. Recommended Values for the Thermal Conductivity of Molten Salts Between the Melting and Boiling Points. *Sol. Energy Mater. Sol. Cells* **2014**, *126*, 11−25.
(22) Gheribi, A. E.; Chartrand, P. Thermal Conductivity of Molten Salt Mixtures: Theoretical Model Supported by Equilibrium Molecular Dynamics Simulations. *J. Chem. Phys.* **2016**, *144*, No. 084506.
(23) Weber, H.; Salanne, M.; Kirchner, B. Toward an Accurate Modeling of Ionic Liquid-TiO2 Interfaces. *J. Phys. Chem. C* **2015**, *119*, 25260−25267.
(24) Haigis, V.; Salanne, M.; Jahn, S. Thermal Conductivity of MgO, MgSiO3 Perovskite and Post-Perovskite in the Earth's Deep Mantle. *Earth Planet. Sci. Lett.* **2012**, *355*−*356*, 102−108.
(25) Gheribi, A. E.; Machado, K.; Zanghi, D.; Bessada, C.; Salanne, M.; Chartrand, P. On the Determination of Ion Transport Numbers in Molten Salts Using Molecular Dynamics. *Electrochim. Acta* **2018**, *274*, 266−273.
(26) Hutchinson, F.; Wilson, M.; Madden, P. A. A Unified Description of MCl3 Systems With a Polarizable Ion Simulation Model. *Mol. Phys.* **2001**, *99*, 811−824.
(27) Madden, P. A.; Wilson, M. 'Covalent' Effects in 'Ionic' Systems. *Chem. Soc. Rev.* **1996**, *25*, 339−350.
(28) Machado, K.; Zanghi, D.; Salanne, M.; Stabrowski, V.; Bessada, C. Anionic Structure in Molten Cryolite-Alumina Systems. *J. Phys. Chem. C* **2018**, *122*, 21807−21816.
(29) Madden, P. A.; Heaton, R.; Aguado, A.; Jahn, S. From First-Principles to Material Properties. *J. Mol. Struct.: THEOCHEM* **2006**, *771*, 9−18. Modelling Structure and Reactivity: the 7th triennial conference of the World Association of Theoritical and Computational Chemists (WATOC 2005).
(30) Tang, K. T.; Toennies, J. P. An Improved Simple Model for the Van Der Waals Potential Based on Universal Damping Functions for the Dispersion Coefficients. *J. Chem. Phys.* **1984**, *80*, 3726−3741.
(31) Ishii, Y.; Salanne, M.; Charpentier, T.; Shiraki, K.; Kasahara, K.; Ohtori, N. A DFT-Based Aspherical Ion Model for Sodium Aluminosilicate Glasses and Melts. *J. Phys. Chem. C* **2016**, *120*, 24370−24381.
(32) Nosé, S. A. Unified Formulation of the Constant Temperature Molecular Dynamics Methods. *J. Chem. Phys.* **1984**, *81*, 511−519.
(33) Martyna, G. J.; Tobias, D. J.; Klein, M. L. Constant Pressure Molecular Dynamics Algorithms. *J. Chem. Phys.* **1994**, *101*, 4177−4189.
(34) Rapaport, D. C. In *The Art of Molecular Dynamics Simulation*; Cambridge University Press: NY, 1996.
(35) Yeh, I.-C.; Hummer, G. System-Size Dependence of Diffusion Coefficients and Viscosities from Molecular Dynamics Simulations with Periodic Boundary Conditions. *J. Phys. Chem. B* **2004**, *108*, 15873−15879.
(36) Salanne, M.; Simon, C.; Turq, P.; Madden, P. A. Conductivity-Viscosity-Structure: Unpicking the Relationship in an Ionic Liquid. *J. Phys. Chem. B* **2007**, *111*, 4678−4684.
(37) Flyvbjerg, H.; Petersen, H. G. Error Estimates on Averages of Correlated Data. *J. Chem. Phys.* **1989**, *91*, 461−466.
(38) Pranami, G.; Lamm, M. H. Estimating Error in Diffusion Coefficients Derived from Molecular Dynamics Simulations. *J. Chem. Theory Comput.* **2015**, *11*, 4586−4592.
(39) Robelin, C.; Chartrand, P. A Density Model Based on the Modified Quasichemical Model and Applied to the NaF-AlF3-CaF2-Al2O3 Electrolyte. *Metall. Mater. Trans. B* **2007**, *38*, 881−892.
(40) Stankus, S. V.; Tyagelsky, P. V. Thermal Properties of Al2O3 in the Melting Region. *Int. J. Thermophys.* **1994**, *15*, 309−316.
(41) Paradis, P.-F.; Ishikawa, T.; Saita, Y.; Yoda, S. Non-Contact Thermophysical Property Measurements of Liquid and Undercooled Alumina. *Jpn. J. Appl. Phys.* **2004**, *43*, No. 1496.
(42) Shpil'rain, E. E.; Yakimovich, K. A.; Tsitsarkin, A. F. Experimental Study of the Density of Liquid Alumina up to 2750.deg. *High Temp. - High Pressures* **1973**, *5*, 191−198.
(43) Rasmussen, J. J. Surface Tension, Density, and Volume Change on Melting of Alumina Systems, Chromia, and Samaria. *J. Am. Ceram. Soc.* **1972**, *55*, No. 326.
(44) Rasmussen, J. J.; Nelson, R. P. Surface Tension and Density of Molten Aluminum Oxide. *J. Am. Ceram. Soc.* **1971**, *54*, 398−401.
(45) Hara, S.; Ikemiya, N.; Ogino, K. Surface Tensions and Densities of Molten Alumina and Titanium Trioxide. *Tetsu to Hagane* **1990**, *76*, 2144−2151.
(46) Langstaff, D.; Gunn, M.; Greaves, G. N.; Marsing, A.; Kargl, F. Aerodynamic Levitator Furnace for Measuring Thermophysical Properties of Refractory Liquids. *Rev. Sci. Instrum.* **2013**, *84*, No. 124901.
(47) Kingery, W. D. Surface Tension of Some Liquid Oxides and their Temperature Coefficients. *J. Am. Ceram. Soc.* **1959**, *42*, 6−10.
(48) Thibodeau, E.; Gheribi, A. E.; Jung, I.-H. A Structural Molar Volume Model for Oxide Melts Part II: Li 2 O-Na 2 OK 2 O-MgO-CaO-MnO-PbO-Al 2 O 3-SiO 2 Melts-Ternary and Multicomponent Systems. *Metall. Mater. Trans. B* **2016**, *47*, 1165−1186.
(49) Lange, R. A. A Revised Model for the Density and Thermal Expansivity of K 2 O-Na 2 O-CaO-MgO-Al 2 O 3-SiO 2 Liquids from 700 to 1900 K: extension to crustal magmatic temperatures. *Contrib. Mineral. Petrol.* **1997**, *130*, 1−11.
(50) Glorieux, B.; Saboungi, M.-L.; Millot, F.; Enderby, J.; Rifflet, J.-C. Aerodynamic Levitation: An Approach to Microgravity. *AIP Conf. Proc.* **2001**, *552*, 316−324.
(51) Elyutin, V. Properties of Liquid Aluminum Oxide. *Fiz. Aerodispersnykh Sist.* **1972**, *57*, 104−109.
(52) Bates, J.; McNeilly, C.; Rasmussen, J. In *Ceramics in Severe Environments*; Springer, 1971; Vol. *5*, pp 11−26.
(53) Bloomquist, R. A.; Fink, J. K.; Leibowitz, L. Viscosity of molten alumina. *Am. Ceram. Soc. Bull.* **1978**, *57*, No. 522.

DOI: 10.1021/acsomega.9b01110
ACS Omega 2019, 4, 8022−8030

(54) Thibodeau, E.; Jung, I.-H. A Structural Electrical Conductivity Model for Oxide Melts. *Metall. Mater. Trans. B* **2016**, *47*, 355−383.
(55) Ansell, S.; Krishnan, S.; Weber, J. K. R.; Felten, J. J.; Nordine, P. C.; Beno, M. A.; Price, D. L.; Saboungi, M.-L. Structure of Liquid Aluminum Oxide. *Phys. Rev. Lett.* **1997**, *78*, 464−466.
(56) Landron, C.; Hennet, L.; Jenkins, T. E.; Greaves, G. N.; Coutures, J. P.; Soper, A. K. Liquid Alumina: Detailed Atomic Coordination Determined from Neutron Diffraction Data Using Empirical Potential Structure Refinement. *Phys. Rev. Lett.* **2001**, *86*, 4839−4842.
(57) Landron, C.; Soper, A.; Jenkins, T.; Greaves, G.; Hennet, L.; Coutures, J. Measuring Neutron Scattering Structure Factor for Liquid Alumina and Analysing the Radial Distribution Function by Empirical Potential Structural Refinement. *J. Non-Cryst. Solids* **2001**, *293*−*295*, 453−457. 8th Int. Conf. on Non-Crystalline Materials.
(58) Florian, P.; Massiot, D.; Poe, B.; Farnan, I.; Coutures, J.-P. A Time Resolved 27Al NMR Study of the Cooling Process of Liquid Alumina from 2450 C to Crystallization. *Solid State Nucl. Magn. Reson.* **1995**, *5*, 233−238.
(59) Poe, B. T.; McMillan, P. F.; Cote, B.; Massiot, D.; Coutures, J. P. Silica-Alumina Liquids: In-Situ Study by High-Temperature Aluminum-27 NMR Spectroscopy and Molecular Dynamics Simulation. *J. Phys. Chem.* **1992**, *96*, 8220−8224.
(60) Coutures, J. P.; Massiot, D.; Bessada, C.; Echegut, P.; Rifflet, J. C.; Taulelle, F. An Aluminum-27 NMR Study of Liquid Aluminates in the 1600−2000 C Temperature Range. *C. R. Seances Acad. Sci., Ser. 2* **1990**, *310*, 1041−1045.
(61) Krishnan, S.; Hennet, L.; Jahn, S.; Key, T. A.; Saboungi, M.-L.; Madden, P. A.; Price, D. L. Structure of Normal and Supercooled Liquid Aluminum Oxide. *Chem. Mater.* **2005**, *17*, 2662−2666.
(62) Jahn, S.; Madden, P. A.; Wilson, M. Transferable Interaction Model for Al_2O_3. *Phys. Rev. B* **2006**, *74*, No. 024112.
(63) Jahn, S.; Madden, P. A. Structure and Dynamics in Liquid Alumina: Simulations with an Ab Initio Interaction Potential. *J. Non-Cryst. Solids* **2007**, *353*, 3500−3504.
(64) Compaan, K.; Haven, Y. Correlation Factors for Diffusion in Solids. Part 2.—Indirect Interstitial Mechanism. *Trans. Faraday Soc.* **1958**, *54*, 1498−1508.
(65) Balducci, A.; Dugas, R.; Taberna, P.; Simon, P.; Plée, D.; Mastragostino, M.; Passerini, S. High Temperature Carbon-Carbon Supercapacitor Using Ionic Liquid as Electrolyte. *J. Power Sources* **2007**, *165*, 922−927.
(66) Shannon, R. D. Revised Effective Ionic Radii and Systematic Studies of Interatomic Distances in Halides and Chalcogenides. *Acta Crystallogr., Sect. A: Cryst. Phys., Diffr., Theor. Gen. Crystallogr.* **1976**, *32*, 751−767.
(67) Kashyap, H. K.; Annapuredy, H. V. R.; Raineri, F. O.; Margulis, C. J. How is Charge Transport Different in Ionic Liquids and Electrolyte Solutions? *J. Phys. Chem. B* **2011**, *115*, 13212−13221.

DOI: 10.1021/acsomega.9b01110
ACS Omega 2019, 4, 8022−8030